



HAL
open science

Coupling hydrological and microclimate models to simulate evapotranspiration from urban green areas and air temperature at the district scale

Timothé Robineau, Auline Rodler, Benjamin Morille, David Ramier, Jérémie Sage, Marjorie Musy, Vincent Graffin, Emmanuel Berthier

► To cite this version:

Timothé Robineau, Auline Rodler, Benjamin Morille, David Ramier, Jérémie Sage, et al.. Coupling hydrological and microclimate models to simulate evapotranspiration from urban green areas and air temperature at the district scale. *Urban Climate*, 2022, 44, pp.101179. 10.1016/j.uclim.2022.101179 . hal-04524035

HAL Id: hal-04524035

<https://hal.science/hal-04524035>

Submitted on 28 May 2024

HAL is a multi-disciplinary open access archive for the deposit and dissemination of scientific research documents, whether they are published or not. The documents may come from teaching and research institutions in France or abroad, or from public or private research centers.

L'archive ouverte pluridisciplinaire **HAL**, est destinée au dépôt et à la diffusion de documents scientifiques de niveau recherche, publiés ou non, émanant des établissements d'enseignement et de recherche français ou étrangers, des laboratoires publics ou privés.



Distributed under a Creative Commons Attribution 4.0 International License

Coupling hydrological and microclimate models to simulate evapotranspiration from urban green areas and air temperature at the district scale

Robineau, Timothé¹ ; Rodler, Auline² ; Morille, Benjamin³ ; Ramier, David⁴ ; Sage, Jérémie⁴ ; Musy, Marjorie² ; Graffin, Vincent⁴ ; Berthier, Emmanuel^{4*}

¹: Andra, DRD-EAP, 1-7 rue Jean Monnet - 92298 Châtenay-Malabry, France
timothe.robineau@gmail.com

²: Equipe de recherche BPE Cerema Nantes, CNRS UMR 5271 - Université Savoie Mont Blanc, Chambéry ; Institut de Recherche en Sciences et Techniques de la Ville (IRSTV), Nantes, France

auline.rodler@cerema.fr, marjorie.musy@cerema.fr

³: SOLENEOS, 1 rue de la Noe – 44200 Nantes, France
benjamin.morille@soleneos.fr

⁴: Cerema, Equipe TEAM, 12 rue Teisserenc de Bort, Trappes, F-78190, France

david.ramier@cerema.fr, jeremie.sage@cerema.fr, emmanuel.berthier@cerema.fr

* Corresponding author, emmanuel.berthier@cerema.fr

Abstract

Understanding and managing hydrological and microclimate conditions is needed for the adaptation of our cities to global warming. Evapotranspiration, or latent heat flux, plays a key role in heat mitigation strategies. Its modelling, as the modelling of its impact on the urban microclimate, remains a scientific challenge, especially during hot periods for which the urban vegetation is subjected to water stress. This article presents an original approach based on the coupling between a hydrological model and a microclimate model to assess the effect of urban green areas on evapotranspiration and air temperatures at the district scale. The approach is applied to a real urban development project, and under future climate conditions. The results show a complex variability of climatic and hydrological behaviour depending on the green zones considered. Results indicate that the water stress control over evapotranspiration can have a significant impact on local surface and air temperatures (respectively 3 to 6°C and 0.6 and 1.6°C difference as compared to ideal water availability conditions).

Keywords

Evapotranspiration, Hydroclimatology, Urban microclimate, Modelling, District scale

1 Introduction

Global warming affects the liveability of our cities during hot periods because of urban characteristics such as building density, anthropogenic heat, material properties, and vegetation cover (Martilli et al., 2020; Oke, 1982). In the past years, many solutions for urban heat mitigation have been investigated among which, nature-based solutions (NBS - they are related to nature: vegetation, waterbodies, soil...), grey solutions (urban forms, materials and technics such as porous pavements, paintings, misting...) and soft solutions (regulation and individual or collective behaviour adaptation). The use of vegetation for urban cooling has been extensively documented, especially the effect of trees shading and evapotranspiration (Gromke et al., 2015; Saaroni et al., 2018; Santamouris, 2014; Shashua-Bar and Hoffman, 2004).

Assessing the cooling effect of vegetation and its impact on comfort at the district scale requires simulating evapotranspiration (ET) and its interaction with surface energy balance and mass flux transport (Tabares-Velasco and Srebric, 2011; U.S. Environmental Protection Agency, 2008). In the literature, most of the microclimate models used to simulate the urban surface energy balance calculate the latent heat flux induced by the vegetation and natural surfaces (Grimmond and Oke, 1991). Water availability at the surface and in the soil is a key parameter to compute the latent heat flux. However, estimating this availability requires water balance calculations, at the surface and in soil, that are not performed or strongly simplified in these models. The Town Energy Balance (TEB) model (Masson, 2000) is one of the few urban climate models that is able to simulate rainfall events (Broadbent et al., 2018; Daniel et al., 2018) at meso-scale. For each type of surface, a water reservoir is set according to the surface water holding capacity and its content is updated at each time step. It is filled during rainfall or watering event and emptied by evaporation. When the maximum capacity of the reservoir is reached, the excess is transferred to the sewer. The hydro-microclimate model TEB-Hydro allows simulating the water and energy budgets with a similar level of detail. Its hydrological component has been improved recently and evaluated (Stavropoulos-Laffaille et al., 2019). However, its impact on the energy component of the model has not yet been investigated and comparison of simulated latent flux with measured data indicates that this term is underestimated. Besides, if this tool is appropriate for large study areas such as a city, its low spatial resolution makes it unsuitable for smaller scale studies.

TheUMEP model (Lindberg et al., 2018) can also be used at a city scale. It is composed of an urban energy and a water balance model. The latter incorporates a single surface reservoir and a single soil reservoir to simulate interception-evaporation and evapotranspiration from the soil for different soil covers depending on water availability. The model computes the infiltration from the surface to the soil reservoir as well as horizontal water movements between the different soil reservoirs. The model has been tested against direct flux measurements: it is able to simulate the net all-wave radiation and the heat fluxes but it was found to underestimate the latent heat flux and to overestimate sensible heat flux in the day time (Järvi et al., 2011). ENVI-met V4¹ model is dedicated to the assessment of microclimate conditions at the district scale. It includes the simulation of surface-plant-air interactions in urban environments. It is designed for microscale domains and allows analysing small-scale (small districts) interactions between individual buildings, surfaces and plants. ENVI-met dynamically computes soil water availability based on Darcy's law, taking into account evaporation, water exchange inside the soil and water uptake by plant roots¹. The main drawback of this tool is that it is based on rectangular meshes, which complicates the representation of slopes as well as urban forms. Besides, the model and the equations

¹ Envi-met. *Basics of Envi-met model* [cited 2018; Available from: <http://www.envi-met.com/introduction/>].

1 involved remain poorly documented, which makes this simulation tool inappropriate for
2 research purposes.

3 Solene-Microclimat is also dedicated to district-scale microclimate simulations with a high
4 resolution (about 1m). It is mainly used to assess the impact of adaptation strategies on
5 outdoor comfort conditions and on buildings energy consumption or indoor thermal comfort.
6 Solene-Microclimat also has the advantage of describing the urban scene in a realistic mock-
7 up, as the urban geometry is implemented in 3D. This tool has been for the most part
8 validated with experimental data and is open access and editable. It considers the interaction
9 between buildings, water ponds, natural or artificial surfaces, and vegetation (Musy et al.,
10 2015). Water stress is however not accounted for. Potential evapotranspiration (PET) is
11 estimated for ideal soil and plant water content conditions. Evapotranspiration can
12 nevertheless be modulated through a ratio between 0 (no evapotranspiration because no
13 water) and 100% (potential evapotranspiration).

14 Hydrological models which often involve detailed water budget calculations during
15 rainy and dry periods, can be used to simulate the water stress of the urban vegetation. Actual
16 evapotranspiration (AET) is traditionally calculated from potential evapotranspiration and a
17 soil moisture extraction function (Berthier et al., 2006; Lingling et al., 2013). PET is defined
18 as the optimal ET rate controlled by microclimate conditions and vegetation properties (Allen
19 et al., 1998), assuming optimum moisture conditions. However, the use of PET formula has
20 several limitations. First, the climatic input they require, such as radiation or air temperature,
21 are usually taken at a reference weather station potentially distant from the studied site. As a
22 result, weather input conditions can be very different from real site conditions that may for
23 instance be affected by the urban heat island (DiGiovanni-White et al., 2018). More generally,
24 meteorological variables governing PET can be highly variable, even at small spatial scales
25 (at the street level for example) (Koelbing et al., 2021). Besides, even with local weather
26 stations, conventional PET calculation approach cannot account for the impact of the
27 surrounding built or natural surfaces that modify shortwave and longwave radiative balance,
28 wind velocity and air temperature: solar shading and solar interreflexions are usually not
29 considered, long wave exchanges between urban surfaces and the vegetation are neglected or
30 simplified, local wind effects are not calculated locally nor measured.

31 Interoperation of hydrology and energy balance appears as a relevant approach to
32 assess the impact of vegetation strategies for urban cooling. This should allow both 1) a better
33 calculation of PET in hydrological models, in which atmospheric conditions would be better
34 represented, 2) a better calculation of AET in urban climate models, considering actual water
35 availability. The objective of this article is thus to introduce a coupling between a
36 hydrological model and the Solene-Microclimat model and to illustrate the benefits of
37 accounting for water availability for evaluating the cooling effect of urban vegetation. The
38 relevance of the approach is assessed on the Paris 2024 Olympic Village case study; the latter
39 aims to investigate the cooling effect of vegetation under future climate conditions.

40 For this article, the microclimatic model is first introduced followed by the hydrologic model
41 and the approach adopted to combine them. Then, the case study of Paris 2024 Olympic
42 Village (OV) project is presented. The results are detailed and discussed afterwards. The AET
43 and PET values for the different high and low vegetal stratum are shown and the impact of
44 considering the real microclimatic conditions is examined. Finally, the importance of
45 accounting for actual evapotranspiration in urban climate simulations is assessed from local
46 climatic outputs.

47

1 2 Materials and methods

2 2.1 Microclimatic model: Solene-Microclimat

3 The Solene-Microclimat model has been developed to investigate the consequences of
4 urban context on local microclimate and indoor thermal conditions of buildings (Musy et al.,
5 2021). It is a freely available open-source code². It is dedicated to the modelling of urban
6 microclimate and building thermal behavior at the district scale. The modelling approach is
7 based on the coupling of radiative, thermal and CFD (Computational Fluid Dynamics)
8 models. The model can simulate a large range of cases encountered in urban projects:
9 modelling of vegetation, soils, building energy simulation, and techniques such as cool paints
10 and surface water aspersion.

11 Solene-Microclimat can be used to evaluate the district heat island and the thermal comfort in
12 open spaces or to compare different urban cooling strategies (use of vegetation, water ponds,
13 materials choices,...) to countermeasure the urban heat island phenomenon. The spatial
14 resolution depends on the meshes generated but is in average about 1m². The simulation can
15 be launched for hourly or sub-hourly time steps. The spatial scale can be the street, square and
16 district, but for thermal comfort studies one of the most important parameter that acts on local
17 climate is the urban form (Leconte et al., 2020). Hence, its explicit description (including
18 buildings, trees, etc.) is a necessary input into microclimate models: Solene-Microclimat is
19 capable of simulating realistic 3D urban settings.

20 The addition of sub-models in Solene-Microclimat makes it possible to take into account: 1)
21 radiative transfers, including long-wave radiation; 2) conduction and storage in walls and
22 soils; 3) airflow and convective exchanges; 4) potential evapotranspiration from natural
23 surfaces like vegetation and water ponds or watering systems; and 5) the energy balance
24 (energy demand or indoor temperature) for a building in the simulated area. Point 1
25 corresponds to the historical SOLENE radiative model and can be run independently.
26 Radiation exchanges consider the beam and diffuse radiation (Miguet, 2000). After having
27 defined the albedo of the surfaces, the interreflexion between surfaces can be calculated for all
28 urban surfaces. Points 1+2 correspond to the thermo-radiative model based on SOLENE
29 (addition of the thermal modelling of different kind of surfaces); it can also be run
30 independently. The thermal model (Bouyer, 2009; Rodler et al., 2018) calculates the thermal
31 exchanges through the walls of buildings or urban surfaces. Points 1+2+3+4+5 correspond to
32 the so-called Solene-Microclimat model (Figure 1). Here, the air movements and the sensible
33 heat fluxes between urban surfaces and air are simulated with code Saturne³. For the moment,
34 the only anthropogenic fluxes simulated by the model are those associated with the heating
35 and cooling of buildings.

36 Different kinds of vegetation can be considered: trees (Robitu, 2005), green roofs and green
37 walls (Malys, 2012) as well as lawn surfaces (Bouyer, 2009). Comparisons have been made
38 by Athamena (2012) on a street canyon composed of containers, showing good agreement for
39 both air temperature and velocity in the street. Besides, all the models used by Solene-
40 Microclimat have been compared independently to measured data.

41

² <https://sourcesup.renater.fr/projects/solenetb/>

³ <https://www.code-saturne.org/cms/documentation/Tutorials>

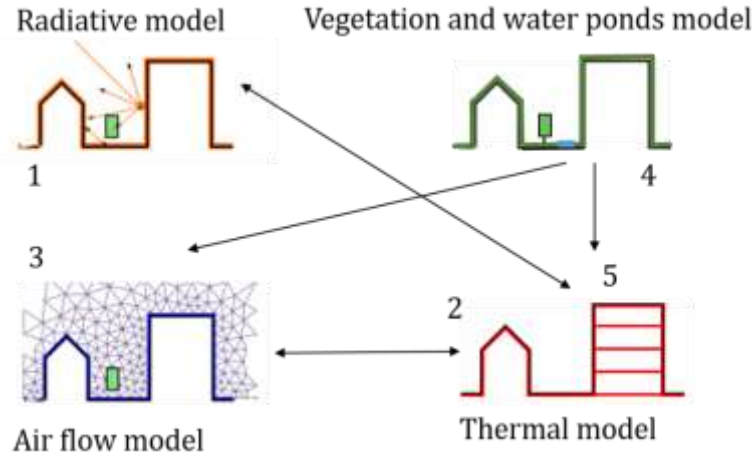


Figure 1: The coupling of the 3 different models included in Solene-Microclimat: Radiative model (1)= SOLENE, Thermal model for urban surfaces(2) and buildings (5), and Airflow model = code-saturne (3). The sub-models (4) locally modify the surfaces and volumes properties in (2) and (5) to represent vegetation and water ponds. Results that are passed from a model to another are represented by arrows, and the green rectangle symbolize a tree.

The primary outputs of the sub-models are their impact on sunlight, wind, air temperature and humidity, and surface temperature.

The ground, roof and wall module included in Solene-Microclimat were previously validated (Musy et al., 2015). The detailed building thermal model performance was assessed too (Rodler et al., 2018), as well as the detailed soil model performance on an open space (a car park) (Azam et al., 2018). Latent fluxes from vegetation and its substrate are used to calculate mass rate of moisture released into the air and taken into account in the CFD model. Malys (2012) performed a first evaluation on green walls with the experimental data recorded by HEPIA, which showed a good agreement. More detail about the case studies and the validation steps can be found in Musy et al., (2021).

This article only provides the equations that have been modified for the coupling and that are related to the latent heat fluxes calculations. The other equations can be found in Musy et al., (2021).

The current version of Solene-Microclimat introduces a ratio AET/PET, denoted as f , to modulate AET : f can be changed on an hourly basis and for each vegetation stratum if specified in an entry file.

For trees, the volumic evapotranspiration for the crown is given below:

$$Ev = \rho_{air} \cdot LAD \cdot \frac{q_{sat} - q_{zref}}{r_{aero} + r_{sto}} \cdot f \quad (1)$$

Where:

Ev is the volumic evapotranspiration rate ($\text{kg m}^{-3} \text{s}^{-1}$)

ρ_{air} is the volumic mass of the air (kg m^{-3})

LAD the leaf area density ($\text{m}^2 \text{m}^{-3}$)

q_{sat} the specific humidity for saturated air at the vegetation stoma level ($\text{kg (water)} \times \text{kg}^{-1}$ (dried air))

q_{zref} the specific humidity at a reference level in the air over the aerodynamic boundary layer of the leaves ($\text{kg (water)} \times \text{kg}^{-1}$ (dried air))

r_{aero} the atmospheric resistance (s m^{-1})

r_{sto} the stomatal resistance (s m^{-1})

The Penman-Monteith equation (Allen et al., 1998) is used to calculate PET for the surface vegetation:

$$PET = \frac{\Delta \cdot (R_n - G) + \rho_a \cdot c_p \cdot \frac{(e_s - e_a)}{r_a}}{\rho_w \cdot \lambda \cdot (\Delta + \gamma \cdot (1 + \frac{r_s}{r_a}))} \quad (2)$$

PET is the potential evapotranspiration (m/s), λ the latent heat of vaporization (J/kg), ρ_w the density of water (kg/m^3), Δ the slope of the saturation vapour pressure temperature relationship ($\text{Pa}/^\circ\text{C}$), R_n the net incoming radiation (W/m^2), G the soil heat flux density (W/m^2), ρ_a the mean air density at constant pressure (kg/m^3), ρ_w the water density at the atmospheric pressure (kg/m^3), c_p the specific heat of the air, $e_s - e_a$ the vapour pressure deficit of the air at a reference level equal to the difference between the saturated vapour pressure minus the actual vapour pressure (Pa), γ the psychrometric constant ($\text{Pa}/^\circ\text{C}$), r_s and r_a the (bulk) stomatal and aerodynamic resistances (s/m). Here, r_s is calculated from leaf area index (LAI) and leaf stomatal resistance values and r_a is estimated from vegetation height (Allen et al., 1998; Bouyer, 2009).

A ratio α_{lat} is introduced to distinguish the water evaporated by leaves and the soil surface, here fixed to 0.5. Latent heat fluxes taken from the vegetation $\varphi_{lat,v}$ and the soil $\varphi_{lat,s}$ nodes are thus computed as follows:

$$\varphi_{lat,v} = \alpha_{lat} \cdot f \cdot PET \quad (3.1)$$

$$\varphi_{lat,s} = (1 - \alpha_{lat}) \cdot f \cdot PET \quad (3.2)$$

The latent heat fluxes for both vegetation strata in Solene-Microclimat depend on climatic variables calculated for each cell of the mesh of the geometry: the solar short wave and long wave radiations, the leaf temperature used for the thermal radiation calculation, the air temperature close to the leaves for the calculation of the saturating vapour pressure, the specific humidity of the air used for the partial pressure calculation of the water vapour, and the wind speed for the calculation of the aerodynamic and stomatal resistances.

2.2 Hydrological model: MARIE

The hydrological model described hereafter is dedicated to the calculation from local climate inputs of AET on urban green areas (typically few m^2 to several thousand m^2) comprising a low (shrubs, grass, perennial plants) and a high (trees) vegetation stratum. The model involves the Penman-Monteith (P&M) equation to estimate PET and relies on a hydrologic scheme, specifically adapted from previous research for this study, to derive AET. The relative simplicity of the model allows performing continuous simulations of the water budget over long-periods (typically one to several years) and thus accounting for the influence of antecedent meteorological conditions on water availability at a given time (Sample and Heaney, 2006).

The use of the P&M equation is generally considered as a reference approach in hydrology for the estimation of evapotranspiration in surface water budget modelling (Broekhuizen et al., 2019; Zhao et al., 2013). Here, the classical expression of the P&M equation presented in previous section (Eq. 2) is used to compute PET over the two vegetation strata. Total PET

1 value applying to simulated green areas is computed as the weighted sum of PET values
2 associated with each stratum, e.g:

$$3 \quad \quad \quad PET(t) = a_{low}PET_{low}(t) + a_{high}PET_{high}(t) \quad \quad \quad (4)$$

4
5 Where: a_{low} and a_{high} represent the area ratio (-) of each stratum ($a_{low} + a_{high} = 1$), $PET_{low}(t)$
6 and $PET_{high}(t)$ PET values calculated for each stratum with the P&M equation.

7
8 The hydrologic scheme adopted to calculate AET from PET is based on a component of the
9 URBS model (Pophillat et al., 2021; Rodriguez et al., 2008). Soil-vegetation profiles are
10 described as a succession of 3 compartments corresponding to i) the interception by the
11 vegetation, ii) the soil surface and iii) the unsaturated zone (UZ). The scheme accounts for the
12 following fluxes: precipitations; evaporation of water intercepted on leaves or branches;
13 runoff from upstream urban surfaces; runoff flowing out simulated green area; evaporation
14 from the soil surface (below vegetation); water flow in the soil; transpiration (e.g. uptake of
15 water by the roots of the vegetation and evaporation by its aerial parts) and exchanges at the
16 bottom of the UZ zone.

17 The original URBS approach relies on the assumption that transpiration from the trees and the
18 lower stratum can be described by an average root extraction function (Rodriguez et al.,
19 2008). In this study, the scheme is adapted to explicitly simulate interception and
20 evapotranspiration for a high and a low stratum sharing the same soil reservoir. This scheme
21 is subsequently referred to as MARIE (Modelling Actual Runoff Infiltration and
22 Evapotranspiration). Its principle is summarized in Figure 2. For each time step, the model
23 successively computes: 1) the water budget in the vegetal interception layer, 2) the transfers
24 within the UZ, and 3) the water budget for the surface layer. Calculations associated with the
25 two surface reservoirs and the UZ are presented hereafter in order to detail the calculation of
26 AET.

27 The URBS model was evaluated for a variety of conditions (Berthier et al., 2020; Jankowsky
28 et al., 2014; Rodriguez et al., 2008) and was found to adequately reproduce the urban water
29 budget, especially its runoff component. The new calculation of water transfers in the UZ was
30 verified against HYDRUS-1D simulations (Simunek et al., 2013) and good agreements were
31 found in terms of soil water content and transpiration fluxes (Pophillat et al., 2021).

1

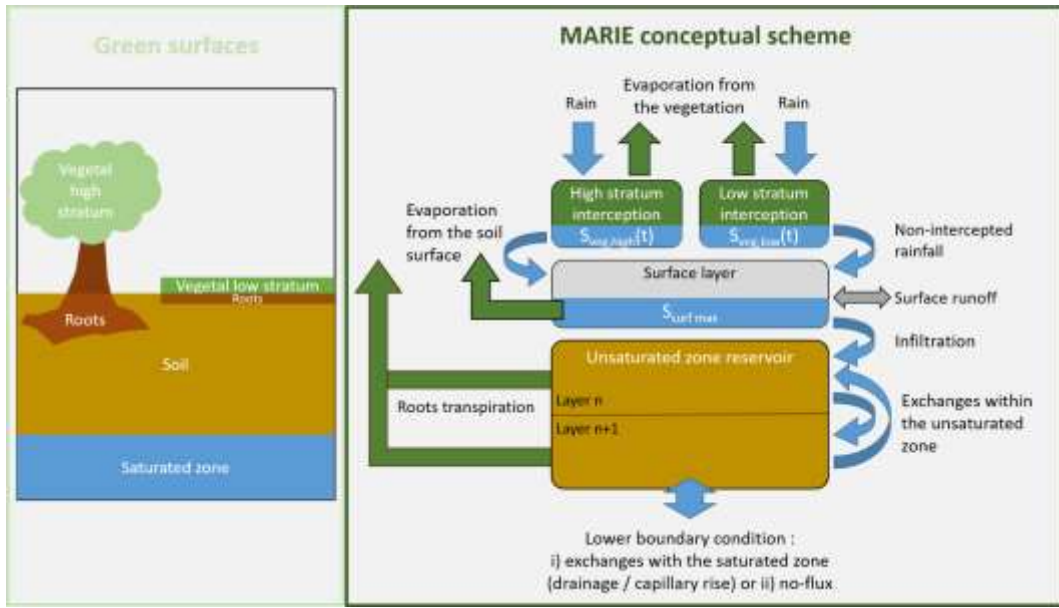


Figure 2: conceptual scheme of the hydrological model MARIE adopted to simulate evapotranspiration from urban green areas

2

3

4

5

6 2.2.1 Vegetation interception reservoirs

7 The first reservoirs describe the interception on the two vegetation strata (Figure 2). For each
8 stratum, the water budget over a time-step (from $t-\Delta t$ to t) is computed as:

9

$$10 S_{veg,s}(t) = S_{veg,s}(t - \Delta t) + P(t) - E_{veg,s}(t) - D_s(t) \quad (5)$$

11

12 With subscript s referring to one of the two strata (low or high), $S_{veg,s}$ the water stored on the
13 vegetation (m), P the rainfall (m), $E_{veg,s}$ the water evaporated from the reservoir (m), and D_s
14 the throughfall (drainage to the underlying surface reservoir) (m).

15

16 Water evaporated by vegetation and throughfall are computed as follows:

17

$$18 \begin{cases} \text{If } S_{veg,s}(t - \Delta t) \leq S_{veg,max,s}: \\ E_{veg,s}(t) = \min\left(\frac{S_{veg,s}(t - \Delta t)}{S_{veg,max,s}} \cdot PET_s(t) \cdot \Delta t, S_{veg,s}(t - \Delta t)\right) \\ D_s(t) = 0 \end{cases} \quad (6)$$

19

$$20 \begin{cases} \text{Else:} \\ E_{veg,s}(t) = \min(PET_s(t) \cdot \Delta t, S_{veg,s}(t - \Delta t)) \\ D_s(t) = a \cdot (S_{veg,s}(t - \Delta t) - S_{veg,max,s}) \cdot \Delta t \end{cases} \quad (7)$$

21

22 With $S_{veg,max,s}$ being the maximum vegetal interception capacity before throughfall occurs (m),
23 PET_s the potential evapotranspiration rate computed at t from the P&M equation ($m \cdot s^{-1}$) and a
24 a drainage parameter (s^{-1}). Note that a specific PET value PET_s is calculated for each stratum
 s to get corresponding $E_{veg,s}$ value.

1 2.2.2 Soil surface reservoir

2 The balance equation of the surface reservoir, shared by the two vegetation strata is written
3 as:

$$4 \quad S_{surf}(t) = S_{surf}(t - \Delta t) + D(t) + R_{in}(t) - E_{surf}(t) - I(t) - R_{out}(t) \quad (8)$$

5
6 Where: S_{surf} is the volume stored at the soil surface per unit area (m), D the cumulative
7 throughfall from the two strata e.g. $D = a_{low} \times D_{low} + a_{high} \times D_{high}$ (m) with D_{low} and D_{high} (m)
8 calculated from Eq. (6) or (7); R_{in} the amount of runoff originating from upstream surfaces
9 that are connected to the green area (m); E_{surf} the evaporation from the surface reservoir (m);
10 I the amount of infiltrated water into the soil (m); R_{out} the amount of runoff flowing out of the
11 green area (m).

12 Here, both infiltration and surface evaporation depend on UZ calculations: the first is limited
13 by the volume the UZ can accept, whereas the second must be adjusted so that AET over the
14 soil-vegetation profile does not exceed PET. The calculation of these two fluxes thus requires
15 UZ budget to be completed (see section 2.2.3). Once the moisture content of the UZ has been
16 updated, I is taken as the minimum between the volume available for infiltration, the storage
17 capacity in the upper UZ compartment and $K_S \times \Delta t$ (where K_S ($m.s^{-1}$) is the saturated hydraulic
18 conductivity of the upper soil layer). The calculation of E_{surf} is detailed in section 2.2.4.

19 At the end of the computation time-step, if surface storage $S_{surf}(t)$ reaches the maximum
20 capacity $S_{surf,max}$, runoff occurs and R_{out} is calculated as $S_{surf}(t) - S_{surf,max}$. Otherwise, R_{out} is set
21 to 0.

22 2.2.3 UZ modelling

23 The conceptualization of the UZ is adapted from Pophillat et al (2021). The UZ is
24 divided in variable thickness layers. Water transfers between layers are calculated using
25 Darcy's law, with the Brooks and Corey (1964) retention curve and hydraulic conductivity
26 functions. The saturated zone (SZ) is not explicitly represented in MARIE, which
27 nevertheless incorporates two options regarding boundary conditions at the bottom of the UZ,
28 e.g., 1) exchanges (recharge, capillary rise) with the SZ computed with Darcy's law or 2) no-
29 flux hypothesis. The water budget of a given layer within the soil profile is given by:

$$30 \quad S_i(t) = S_i(t - \Delta t) + (q_{i-1,i}(t) - q_{i,i+1}(t)) \cdot \Delta t - Tr_i(t) \quad (9)$$

31
32 Where: S_i is the water storage in layer i (m), $q_{i-1,i}$ the flux from layer $i-1$ to layer i calculated
33 by Darcy's law or selected in accordance with boundary conditions ($m.s^{-1}$), and Tr_i
34 transpiration in layer i (m). Whereas the original URBS scheme considers a single root
35 system, transpiration Tr_i here represents the cumulative contribution of the low and high
36 vegetation strata ($Tr_{i,low}$ and $Tr_{i,high}$). Tr_i is thus calculated as a weighted average over these
37 two components, e.g. $Tr_i = a_{low} \times Tr_{i,low} + a_{high} \times Tr_{i,high}$.

38 The calculation of each transpiration component is based on the Feddes et al. (1978) model.
39 Total transpiration Tr (m) applying to the UZ over a time-step is given by:

$$40 \quad Tr(t) = \sum_{\substack{s \in \\ [low,high]}} a_s \cdot \left[E_{d,s}(t) \cdot \sum_{i=n}^N dr_{i,s} \cdot \min \left(\frac{\psi_i(t - \Delta t) - \psi_{WP}}{\psi_{FC} - \psi_{WP}}, 1 \right) \cdot \Delta t \right] \quad (10)$$

41

1 With: a_s the area ratio for vegetation stratum s (low or high); $dr_{i,s}$ the root density in layer i (-)
 2 for vegetation stratum s , ψ_i the pressure head in layer i , ψ_{WP} the pressure head at the wilting
 3 point e.g. -150 m, ψ_{FC} = pressure head at field capacity e.g. -3.3 m and $E_{d,s}$ the evaporative
 4 demand ($m \cdot s^{-1}$) calculated as $PET_s(t) - E_{veg,s}(t)/\Delta t$ for each vegetation stratum. Note that the
 5 term within the brackets is the transpiration $Tr_{,s}$ (m) associated with the stratum s .

6 2.2.4 AET calculation

7 The (mean) AET from the green area is finally calculated as the sum of
 8 evaporation/transpiration terms applying to the vegetation-interception reservoir, the soil
 9 surface and the UZ:

10

$$AET(t) = E_{veg}(t) + E_{surf}(t) + Tr(t) \quad (11)$$

11

12 Where: E_{veg} is the cumulative evaporation from the vegetation reservoirs e.g. $E_{veg} = a_{low} \cdot$
 13 $E_{veg,low} + a_{high} \cdot E_{veg,high}$, with $E_{veg,low}$ and $E_{veg,high}$ calculated from Eq. (6) and (7).

14 The value of $E_{d,s}$ in Eq. 10 ensures that the sum of evaporation from vegetation surface $E_{veg,s}$
 15 and transpiration $Tr_{,s}(t)$ does not exceed $PET_s(t)$ over the low and high strata. Similarly,
 16 surface evaporation E_{surf} is adjusted so that $AET(t)$ remains smaller than or equal to $PET(t)$:

17

$$E_{surf}(t) = \min(S_{surf}(t - \Delta t) + D(t) + R_{in}(t) - I(t), PET(t) - E_{veg}(t) - Tr(t)) \quad (12)$$

18

19 As explained in 2.2.1, $I(t) \leq S_{surf}(t - \Delta t) + D(t) + R_{in}(t)$ so that infiltration never exceeds the
 20 volume available in the surface reservoir. This in turn implies that $E_{surf} \geq 0$ in Eq. (12).

21 Note that AET values associated with each stratum s can be computed from Eq. 11 using $E_{veg,s}$
 22 and Tr_s for E_{veg} and Tr .

23

24 2.3 Coupling microclimatic and hydrologic models

25 Due to differences in spatial and temporal discretizations and simulation period
 26 requirements for each model (one year for MARIE and a dozen of days for Solene-
 27 Microclimat), the two models operate independently and the exchange of data is done
 28 manually. The coupling is carried out in three steps to simulate the urban microclimate
 29 considering water availability on urban green areas (Figure 3):

30

1) solar radiation calculations are first conducted with Solene-Microclimat,

31

2) local radiation conditions derived from these calculations are then used to compute

32

PET and to simulate AET with MARIE,

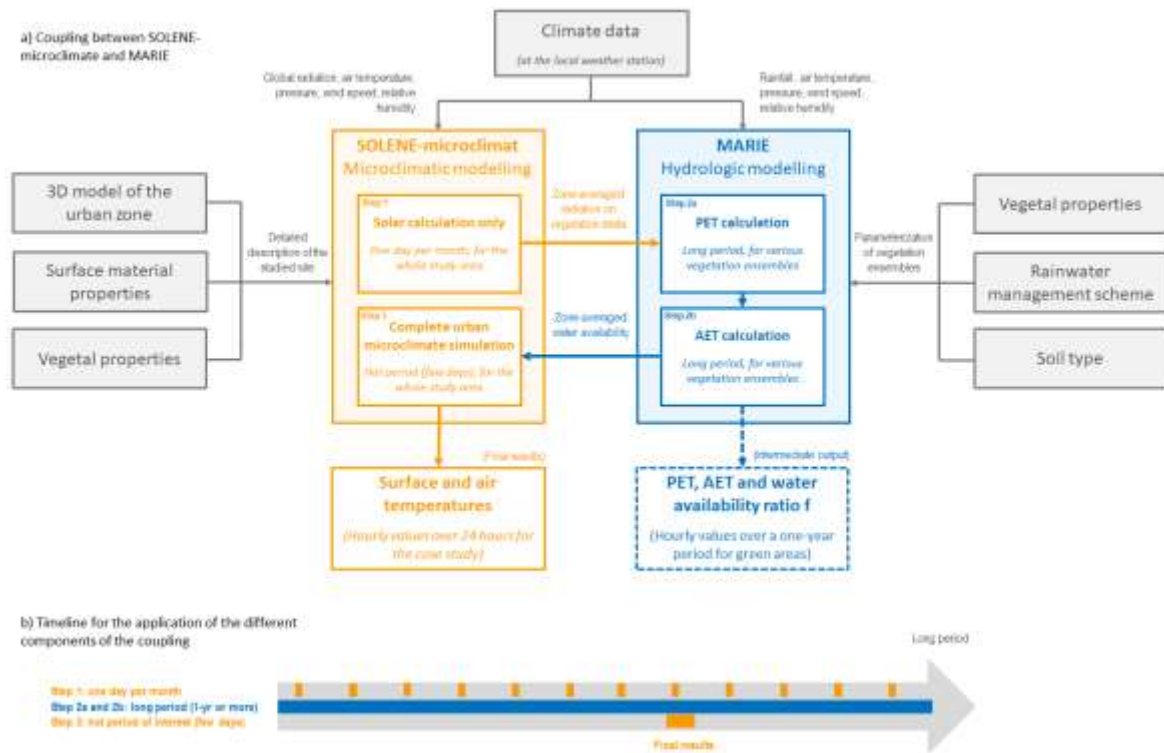
33

3) values of the ratio f between AET and PET calculated by MARIE are adopted by
 34 Solene-Microclimat to perform complete microclimate simulations that provide surface and
 35 air temperatures over the studied area.

36

37 Each of the three steps described above involves different modelling scales. Solar radiation
 38 calculations rely on a full 3D discretization of the studied area. Next, several green zones are
 39 identified for the estimation of AET and water availability. These zones are themselves
 40 subdivided in homogeneous vegetation subzones (including a low and high stratum, cf.
 41 section 2.5.1) with their own characteristics. Average radiation values associated with low and
 42 high vegetation strata are computed for each of them. Hydrological simulations are conducted
 43 for each vegetation subzones and averaged water availability ratio f are later derived for each

1 zone. These ratio are finally used to constrain the behaviour of vegetated surfaces in the
 2 detailed microclimate modelling.
 3



4
 5 *Figure 3: Procedure for the coupling between the microclimate and hydrological models: a) description of the different*
 6 *elements and steps of the coupling, b) corresponding timeline*

7
 8 The timeline in figure 3 shows the temporal scales involved at each step of the coupling
 9 approach. Due to the time of calculation and interpretation, the microclimate simulation
 10 period is limited to a few weeks, generally including a hot period of interest. In contrast,
 11 hydrological simulation must be conducted over a long period (typically 1-yr) to describe the
 12 evolution water availability and properly account for the effect of antecedent meteorological
 13 conditions during this hot period of interest. Climate input associated with the 2 models are
 14 listed in figure 3 (details regarding the time series used in this article can be found in 2.4.2).
 15 The solar radiation used by MARIE is generated with Solene-Microclimate based on a
 16 simplistic approach: simulations are conducted for a single day for each month, considering
 17 the shading of buildings but not the transmission through trees nor the interactions with the
 18 urban scene; the ratio between solar radiation with and without shading for this day is then
 19 applied for each day of the month to produce the long-period solar radiation input needed in
 20 MARIE.

21 2.4 Case study

22 The relevance of the combination of hydrologic and microclimatic modelling
 23 approaches is illustrated on the Paris 2024 Olympic Village (OV) project. The application
 24 focuses on the evaluation of evapotranspiration, surface and air temperatures in future site and
 25 climate conditions.

2.4.1 Site description

The OV (0.3 km²) will be constructed along the Seine River between the Saint-Ouen and the Saint-Denis cities (Île-de-France region). For this article, simulations focus on the “Mail Finot”, a 51 700 m² landscaped plaza lane going down to the Seine River. The Mail Finot, expected to be a frequented public space, is of interest for microclimate simulations because of the presence of numerous vegetated surfaces which may impact the local urban climate. The composition of these surfaces is accounted for in microclimate and hydrological simulations and presented in Figure 4. The Mail Finot is subdivided in 5 green zones: zone 1 is a vegetated passage between buildings, zone 2 groups trees and planters implanted on concrete pavers, zone 3 and zone 4 correspond to the largest vegetated area of the Mail Finot (with denser vegetation in zone 4), and zone 5 is a ruderal Elm forest located near the Seine River.



14
15

Figure 4: Vegetation types on the 5 zones studied on the Olympic Village project

2.4.2 Simulation periods and meteorological data

The evaluation of evapotranspiration, surface and air temperatures is conducted for future climate conditions, under a possible and severe scenario. Météo-France (French national meteorological service) provides ensembles of meteorological data for 2050 at a hourly time-step, following the IPCC-RCP8.5 scenario (IPCC, 2014). Here, a particularly hot year (3rd hottest quartile among the 200 “2050” simulations) is selected for the application. As explained in 2.3, the modelling approach involves different timescales. Solar radiations are calculated with Solene-Microclimat on the Mail Finot for one typical day of each month of the 2050 hot year from hourly global radiation values. Hydrological modelling is performed over the whole year from hourly meteorological data to derive PET and AET time-series. Microclimate modelling is finally conducted over a particularly hot 12-days period ranging from 26th August to 6th September (and focuses on 2nd September for the presentation of the results). The characteristics of the 2050 hot year and the associated hot 12 days period are summarized in Table 1. Climate conditions of 2018-2019 years are also shown for

1 comparison in Table 1, including characteristics of the same 12 days period from 26th August
 2 to 6th September of 2018 and 2019 (these periods are not the hottest of 2018 and 2019 but
 3 nonetheless illustrate current climate conditions during summer periods).
 4

	2050 hot year		2018-2019	
	Whole year	Hot 12 days period	Whole year	Same 12 days period
Cumulative rainfall (mm)	684	4	697	8
¹ Air temperature (°C)	16.1 [0.1; 41.6]	30.1 [19.8; 41.6]	12.9 [-8.5;41.2]	18.8 [6.1;33.1]
¹ Relative humidity (%)	51 [2; 78]	24 [2; 64]	72 [15; 99]	62 [27; 94]
¹ Wind speed (m/s)	3.5 [0.2; 15.4]	2.7 [0.6; 7.2]	3.5 [0;15.7]	2.6 [0;7.7]
¹ Solar radiation (W/m ²)	129 [0; 948]	212 [0; 664]	136 [0; 978]	181 [0;778]

5 *Table 1: Climate characteristics of the 2050 hot year and corresponding hot 12 days period considered in the application of*
 6 *the modelling approach, and comparison with actual climate (mean of 2018 and 2019) (¹Mean value and [min; max] based*
 7 *on hourly values)*

8 The 2050 hot year exhibits higher mean air temperatures (+3°C) and a significantly lower
 9 mean relative humidity (-20%) than the 2018-2019 period. These differences are exacerbated
 10 during the summer period. Mean solar radiation and cumulative rainfall remain similar,
 11 although the distribution of rainfall differs.

12 2.5 Model parameterization

13 2.5.1 Penman-Monteith equation

14 Parameters of the P&M equation have been compiled from the literature (Breuer et al.,
 15 2003; Eermak, 1998; Eliáš, 1979; Gyeviski et al., 2012; Miller et al., 2020; Samson et al.,
 16 2005; Wang et al., 1995) and used in this study to characterize the main vegetal species of the
 17 5 vegetation zones of the Mail Finot. Each zone may include a variety of high and low
 18 vegetation types (Figure 4). “Low stratum + high stratum” vegetation subzones are first
 19 constructed by grouping together areas sharing the same low vegetal stratum (for instance,
 20 trees located above turf fall within the same vegetation subzone as turf cover). For each
 21 subzone, vegetation parameters associated with the low and high strata are set in accordance
 22 with the values found in the literature. Average values of these parameters over the 5 green
 23 zones are presented in Table 2.

24 Table 2 also displays net radiations corrected from trees and buildings shadings for both
 25 vegetal strata (see 2.3.1). Because of tree height, high vegetal strata receive higher amounts of
 26 solar radiation than low strata which are partly shaded by trees and buildings.

27 2.5.2 Hydrological flow routing within the studied area

28 Assumptions regarding the routing of runoff across the studied area are needed to
 29 compute the upstream surface runoff of each zone, e.g. the R_{in} term in Eq. 8. The surfaces
 30 feeding the 5 green zones (located upstream the Mail Finot) are delimited from the
 31 stormwater management plan of the OV project and characterized by a mean runoff
 32 coefficient C (-). The latter is adjusted in accordance with soil cover (concrete, pavers, grass).
 33 The area of these upstream surfaces and corresponding runoff coefficient can be found in
 34 Table 2, and the incoming runoff term R_{in} (m) is simply computed as:

$$35 \quad R_{in}(t) = C \times P(t) \times S_{up}/S_{zone} \quad (13)$$

36 Where S_{up} is the area of the upstream surface (m²) and S_{zone} the area of the green zone (m²).
 37

2.5.3 Hydrological parameterization of the soil-vegetation profile

The extension of the UZ below the Mail Finot varies along the five green zones, depending on their distance to the Seine River. As opposed to the four other zones, zone 2 consists of tree plantation pits and is thus disconnected from the groundwater. Its thickness corresponds to the depth of tree plantation pits and a no-flux boundary condition is set at its bottom. Zone 4 is subdivided in two parts because of a significant UZ thickness contrast between the upstream part and the hillside part near to the Seine River. The detail of UZ extensions and boundary conditions for each zone can be found in Table 2.

Hydrological parameters associated with the interception and surface reservoirs are set in accordance with the values mentioned in the literature (Grimmond and Oke, 1991; Rodriguez et al., 2008): $S_{veg,max}$ is equal to 1.3 mm from April to September and 0.3 mm from October to March; a to $0.04 \text{ (s}^{-1}\text{)}$; and $S_{surf,max}$ to 1 mm.

For each green zone, the following discretization is adopted: the first metre of the UZ is divided in five 20 cm layers and 50 cm layers are used from the first metre to the bottom of the soil column. Based on available field measurements, the UZ is described as a homogeneous silt column. Corresponding hydrodynamic parameters are those provided by Rawls et al. (1982).

Specifying root distribution is required to simulate transpiration with MARIE. Three subgroups are considered for the low vegetation stratum: root depth is set to 20 cm for grass and undergrowth; 40 cm for perennials and vegetal mix of gardened passages; and 80 cm for vegetal mix of forest edges (the low stratum of the different vegetation subzones over which AET is computed falls within one of these three subgroups). The depth of tree root systems is set to 2 m. For both strata, roots are assumed to be equally distributed within the root profile (homogeneous root density).

	Zone 1		Zone 2		Zone 3		Zone 4		Zone 5	
Area (m ²)	1700		1400		1800		3900		1400	
Vegetation parameters and solar radiation (2.5.1)										
Strata	High	Low	High	Low	High	Low	High	Low	High	Low
Surface	840	820	1400	330	700	1100	1900	1900	1300	120
LAI (-)	4.0	3.0	6.0	3.0	4.2	2.9	4.4	2.9	4.5	3.0
rs (s/m)	80.7	101.0	89.1	101.0	101.4	50.8	90.7	61.4	105.9	87.9
hveg (m)	13.1	0.7	15.6	0.5	16.3	0.3	21.1	0.8	20.0	1.6
Rn (W/m ²)	50.3	38.0	61.3	36.6	64.8	57.8	74.1	57.2	99.1	38.0
Flow routing information (2.5.2)										
Upstream runoff surface (m ²)	2500		0		4900		5800		0	
Runoff coefficient (-)	0.8		/		0.5		0.5		-	
UZ parameterization (2.5.3)										
UZ thickness (m)	13		3		16		14 / 9		9	
Lower boundary conditions	Darcy's law		No-Flux		Darcy's law		Darcy's law		Darcy's law	

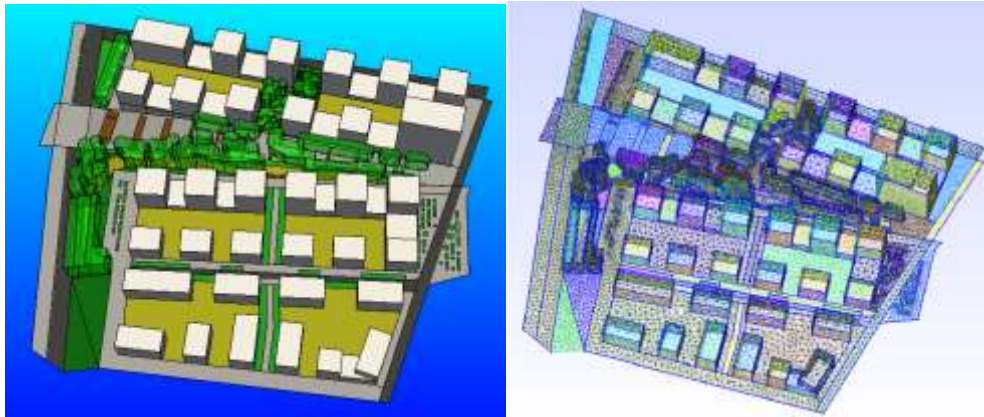
Table 2: Summary of the characteristics and parameterization of the 5 green zones

2.5.4 Mock-up of the Mail Finot

The district around the Mail Finot has been built by considering buildings footprint and volume, ground topography, the delimitation of the different zones studied and the

1 representation of the vegetation (location/footprint, volume of the crown for trees and all
 2 characteristics having impact on the evapotranspiration phenomenon). The Mail Finot mock-
 3 up is composed of 97698 surface meshes for all the urban area (Figure 5). However, the
 4 thermal exchanges are calculated on 42808 surface meshes only. The meshes generated on the
 5 urban surfaces guide the generation of the 3D volumic meshes, which leads to 462517
 6 volumic tetrahedrons in total. Details regarding the thermal and radiative properties on the
 7 mock-up can be found in the Appendix.

8



9
 10 *Figure 5: Mail Finot's mock-up on left, and Meshing of the mock-up on right*

9
 10

11 3 Results

12 3.1 Coupling simulations results

13 3.1.1 Variability of solar radiation on green zones

14 Solar (or short wave) radiation is one of the key drivers creating overheating in urban
 15 areas.

16 The variability of solar radiation can first be examined based on mean solar radiation
 17 values received by each zone. The latter are calculated from hourly solar radiation simulated
 18 by Solene-Microclimat during the 2050 year and shown in table 3. The low stratum receives
 19 less radiation than the high stratum due to the shading of trees and buildings. Zone 5 receives
 20 the highest radiation flux because this zone is not shaded by the surrounding buildings.

21
 22

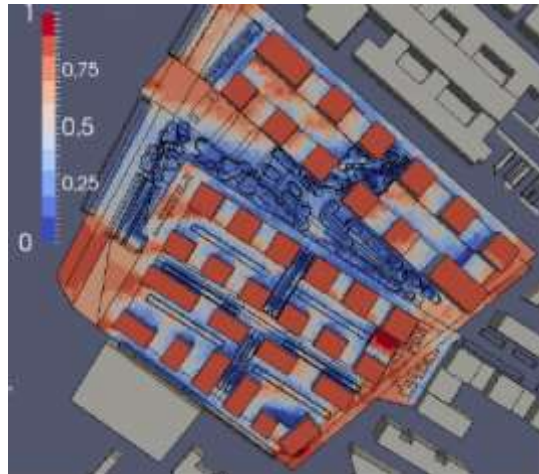
Vegetation stratum	Zone 1	Zone 2	Zone 3	Zone 4	Zone 5	Without shading
High stratum	65	80	84	96	129	129
Low stratum	49	47	75	74	84	129

23 *Table 3: Mean values (year 2050) of the solar radiation received by each zone affected by the buildings and trees shading*
 24 *(in W/m²)*

25 Final solar simulations (Step 3 in Figure 3) not only take into account the differences
 26 associated with shading but also consider the interactions between solar rays and the urban
 27 scene. When solar radiation reaches the urban surface:

- 28 - a part of the flux is absorbed, depending on the absorption coefficient,
- 29 - another part is transmitted (for buildings windows or tree crown) depending on the
 30 surface's transmission coefficient,
- 31 - and the complementary part is reflected, depending on the albedo.

1 The reflected part can reach other surfaces and be also absorbed, transmitted and again
 2 reflected. In a second approach, an insolation indicator is calculated to characterize the
 3 radiation received by each zone. For each zone, the cumulated radiation received by the lower
 4 stratum during the hours of solar exposition is calculated. This value is then normalized by the
 5 cumulated radiation received during the same period by a horizontal surface with no obstacle
 6 (e.g. maximum value). This normalized cumulated radiation is presented in Figure 6 and
 7 Table 4 during one particular sunny day: for example, for zone 1, 16% only of the total
 8 radiation received with no obstacles or shading reaches the lower stratum.
 9



10
 11 *Figure 6: Normalized cumulated solar radiation for the 2nd Sept 2050 around the Mail Finot*

12

	Mean number of hours of solar radiation	Normalized cumulated mean solar radiation
Zone 1	3.3	16%
Zone 2	6.7	20%
Zone 3	3.7	23%
Zone 4	7.5	19%
Zone 5	9.2	27%

13
 14 *Table 4: Hours of radiation and cumulated mean solar radiation of the lower stratum on the green zones for the 2nd Sept 2050*

15 Zone 1 has a low exposition to solar radiation, during the year and the hot period studied, and
 16 the trees don't affect much this low level as the surrounding environment is already creating
 17 solar masks. On the contrary, zone 5 is well exposed to the sun, despite trees that affect the
 18 radiation on the ground due to their shading. Zones 2 and 4 show contrasting conditions at the
 19 annual scale but similar ones during the hot period with an important time of solar radiation
 20 and rather low cumulated mean radiation. Zone 3 has a low time of solar radiation but stays
 21 well exposed during this time and with a low effect of trees.

22 **3.1.2 Evapotranspiration on green zones**

23 MARIE simulates PET and AET at an hourly timestep over the whole year 2050 for
 24 each of the green zones studied. The ratio f between AET and PET is used as an indicator of
 25 vegetation water stress.

26 The average PET value for year 2050 across the 5 zones is high (Table 5): 1125mm in
 27 comparison with 687mm under current climate and corresponding 650 mm rainfall. The
 28 values are rather homogeneous between the zones, with a maximum difference of 10%
 29 between zones 4 and 1. However these averaged values of PET hide a variability between low

1 and high strata within the zones. Zones 1 and 2 exhibit the maximum discrepancy with PET
 2 30% higher for high strata than for low strata (for zone 1 (resp. zone 2) annual PET for year
 3 2050 is 1264 mm (resp. 1204 mm) for the high stratum and 879 mm (resp. 848 mm) for the
 4 low stratum). Comparatively, for zone 5, PET remains similar between the two strata, with
 5 around 1086 mm for the year 2050. PET values can be explained by net radiation and
 6 vegetation characteristics (see Eq.2). Zone 5 low stratum receives the same amount of net
 7 radiation (38 W/m² in annual average) as zone 1 low stratum but has an about 20% higher
 8 PET value. On the contrary, zone 5 high stratum receives the maximum amount of net
 9 radiation (99 W/m² in annual average) but shows one of the weakest high strata PET. The
 10 high stratum of zone 1, for example, has a 13% higher PET with half of the net radiation. In
 11 this case study, the main factors controlling the variability of annual PET values are thus the
 12 characteristics of the vegetation and not the micro-meteorological conditions.
 13

Variables	Zone 1		Zone 2		Zone 3		Zone 4		Zone 5	
	2050 year	2050 hot period								
PET (mm)	1067	94	1120	102	1169	91	1186	99	1086	104
AET (mm)	1019	81	980	70	1053	57	978	50	739	35
PET-AET (mm)	48	13	140	32	116	34	208	49	347	69
AET/PET (-)	0.96	0.86	0.88	0.69	0.90	0.63	0.82	0.51	0.68	0.34

14 *Table 5: Potential and actual evapotranspiration for each zones of the Mail Finot (cumulated values during the year and the*
 15 *hot period studied)*

16 Average cumulated AET is strongly variable from one zone to another (Table 5 and
 17 Figure 7) but shows the same pattern as PET across the strata within each zones. Higher AET
 18 difference between high and low strata is observed for zone 1 (1221 mm for high stratum
 19 instead of 830 mm for low stratum) and zone 3 shows the most homogenous values (1033 mm
 20 for high stratum and 1088 mm for low stratum).
 21

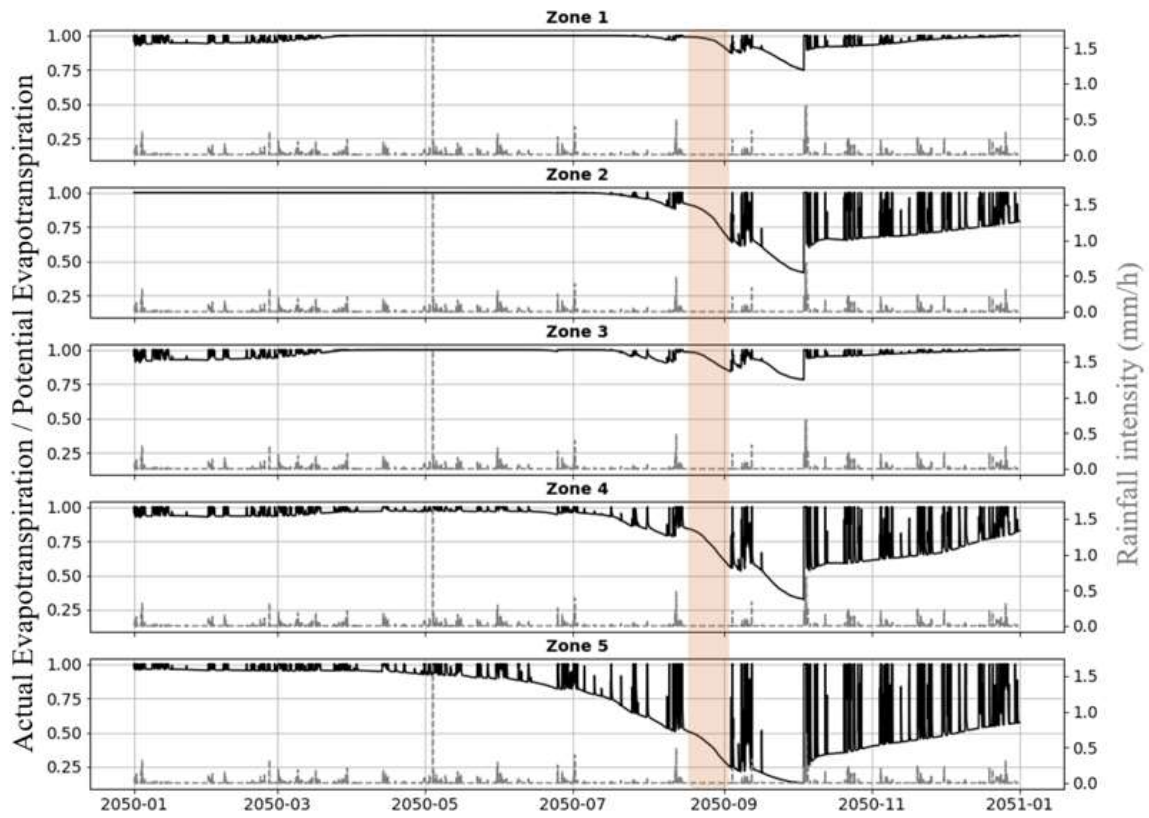
22 On zone 1, the difference between PET and AET is low (4% for the year, and 14% during the
 23 hot period) because the soil water content stays relatively high, even during dry periods ; this
 24 high soil humidity is mainly explained by the large upstream runoff surface connected to this
 25 zone (Table 2). The AET of zones 2, 3 and 4 are limited in comparison with PET. Green areas
 26 of zone 2 receive no upstream runoff but the no flux condition at 3 m depth (Table 2) allows
 27 retaining enough water to feed the soil and the vegetation during the hot period. Vegetation of
 28 zones 3 and 4 are significantly more stressed during the hot period due to a deeper saturated
 29 zone. Finally, the most AET limited zone is zone 5, with value of 739 mm for the year and
 30 only 35 mm during the hot period, representing respectively 68% and 34% of the PET values.
 31 This behaviour is mainly due to the high stratum that can only evaporate 66% of the annual
 32 PET (90% for low stratum). The combination of an absence of runoff from upstream surfaces
 33 and a relatively large distance to the water table explains this significant water stress, which
 34 appears in May and lasts all the year, including very low value of AET/PET during all the
 35 summer season.
 36

37 A more detailed examination of AET dynamics confirms the differences in the behaviour of
 38 vegetation strata (Figure 7). The low vegetation can be severely stressed during periods with
 39 strong heat waves, with a near-zero evapotranspiration on some zones (not shown), but almost
 40 evapotranspirates at the potential value during the rest of the year (with usual rainfall and
 41 limited potential evapotranspiration). High vegetation strata show higher annual AET/PET
 42 ratios, except for zone 5, but undergo water-stress for a longer period with lesser intensity (see

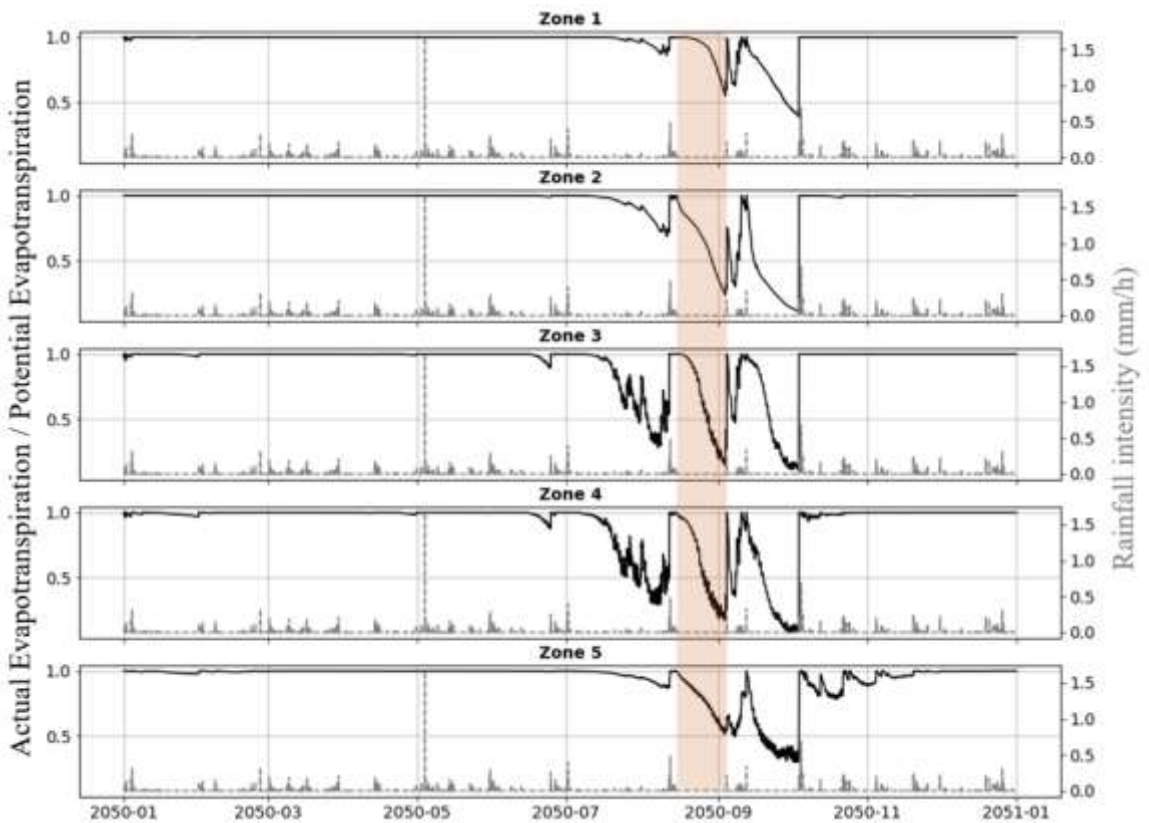
1 the numerous and short rises appearing in the high vegetation curve of Figure 7). Low stratum
2 is thus more affected by long dry and hot periods but is able to capture most of the infiltrated
3 volume during rain events that do not reach the tree roots except for heavy rainfall.

4 The simulation performed with MARIE indicates that soil water content is an
5 important determinant of evapotranspiration on the green zones of the Mail Finot, that
6 frequently and significantly limits this flux, especially during heatwave and dry periods.
7 Considering AET instead of PET for microclimate simulation is thus justified in this case
8 study.

9



(a)



(b)

Figure 7: Spatial and temporal evolution of the water stress in the Mail Finot (for high (a) and low (b) vegetal stratum of each green zone during the 2050 year; the red underlined column indicates the hot period studied)

1

2

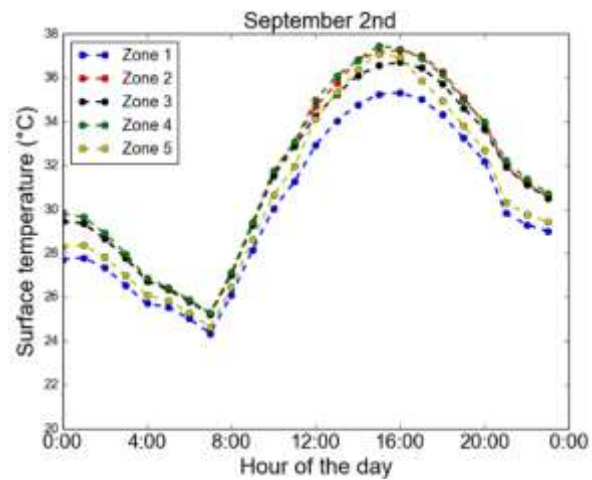
3

4

5

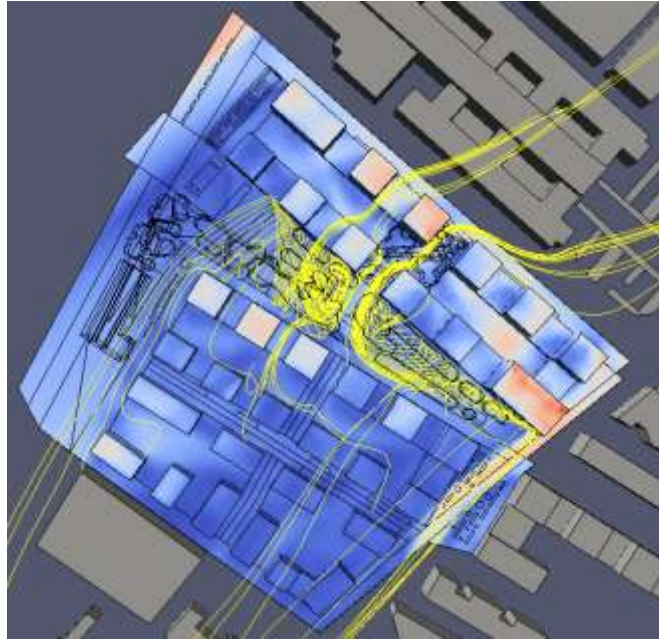
1 3.1.3 Surface and air temperature

2 Here, the ratio f between AET and PET calculated for each hour by MARIE is used as
3 an input to Solene-Microclimat, for both the high and low vegetation stratum of each zone.
4 The surface temperatures are impacted by several factors: the nature of the soil cover and its
5 composition, the exposition to solar radiation, the wind intensity and direction, the thermal
6 exchanges through the materials, and the latent heat flux. The mean surface temperature
7 evolution of each zone on the 2nd September is shown on Figure 8. Each green zone
8 temperature has a different evolution: zone 1 has the coolest surface temperature, due to its
9 low exposition to solar radiations; zones 2 and 4 have the highest surface temperature
10 followed by zones 3 and 5. The maximum values, between 34 and 38°C, stay relatively low
11 due to the latent heat fluxes at the surface of the green zones.
12



13
14 *Figure 8: Mean surface temperature for each green zone for the 2nd Sept 2050*

15 The air temperatures are influenced not only by the surface temperatures through the latent
16 heat but also by the wind direction and intensity. It has to be noticed that the results shown in
17 this article are dependent on the wind conditions prescribed at the limit of the mock-up (wind
18 intensity of 2.7 m/s coming from north-east) and different conditions would probably lead to
19 different results. In the Mail Finot, the five green zones are exposed to a wind that doesn't
20 exceed 2m/s: zone 1 is the most exposed with a mean wind velocity of 1.8 m/s, with wind
21 flowing from adjacent buildings (Figure 9); zone 2 has a mean wind velocity of 1.1 m/s, zone
22 3 of 1.4 m/s, zone 4 of 0.8 m/s and zone 5 of 1.4 m/s. The air mass going out of zone 1 moves
23 on to the rest of the Mail Finot, with recirculation occurring first in the middle of the
24 promenade, showing low wind intensities. The wind then moves on to the more mineral areas
25 downstream, but these air masses do not move on to the south-oriented zones like zone 5.

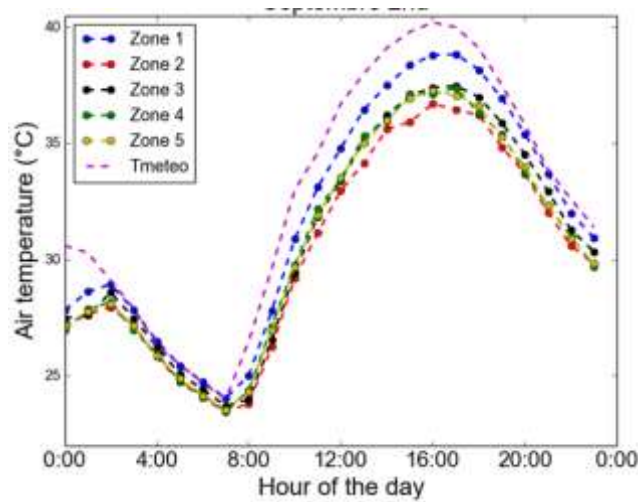


1
2

Figure 9: Power line of the wind through the mail Finot for the main direction and wind intensity as input

3 Overall, air temperatures in the mail Finot are lower than upstream or than the one measured
 4 by the weather station (Tmeteo, Figure 10): the maximum can reach 34-39°C during the 2nd of
 5 September, where the upstream temperature exceeds 40°C. Due to the wind circulation, zone
 6 1 is not much cooled down, as the air mass is not for a long time in contact with the vegetated
 7 surfaces. At the exit of zone 1, close to the mail Finot promenade, the air is warmer than on
 8 the remaining part of the Mail Finot, as on these zones the air is cooled down by the
 9 vegetation (Figure 11).

10



11
12
13

Figure 10: Mean air temperature above each green zone for the 2nd Sept 2050 (the pink dashed line is for the weather station)

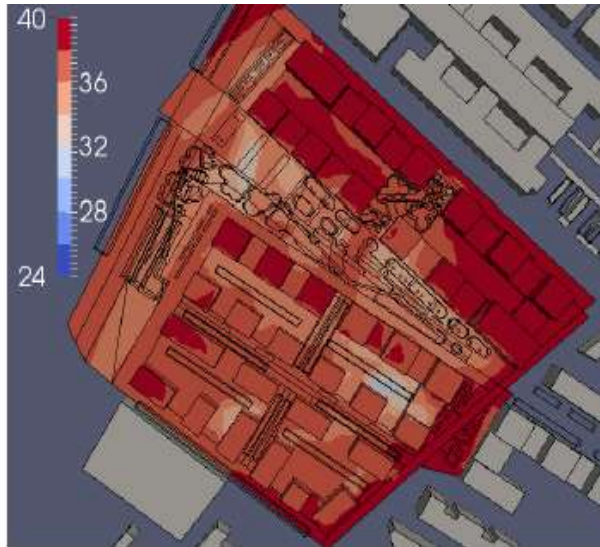


Figure 11: Air temperature maps at 2pm the 2nd Sept 2050

3.2 Impact of accounting for actual evapotranspiration on micro-climate

This paragraph presents the comparison of previous surface and air temperature results with those obtained using PET instead of AET values in the Solene-Microclimat (f=1). For the maximal water availability configuration, zones 1, 2 and 5 exhibit the highest mean surface temperature (Figure 12); zones 3 and 4 show lower mean temperatures thanks to large surfaces of lawn that are cooler than the perennial plants or the forest borders.

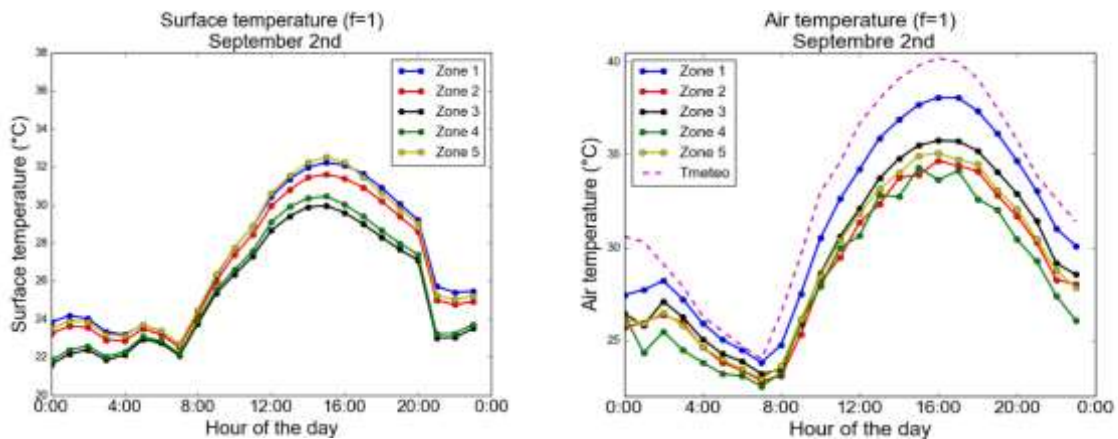
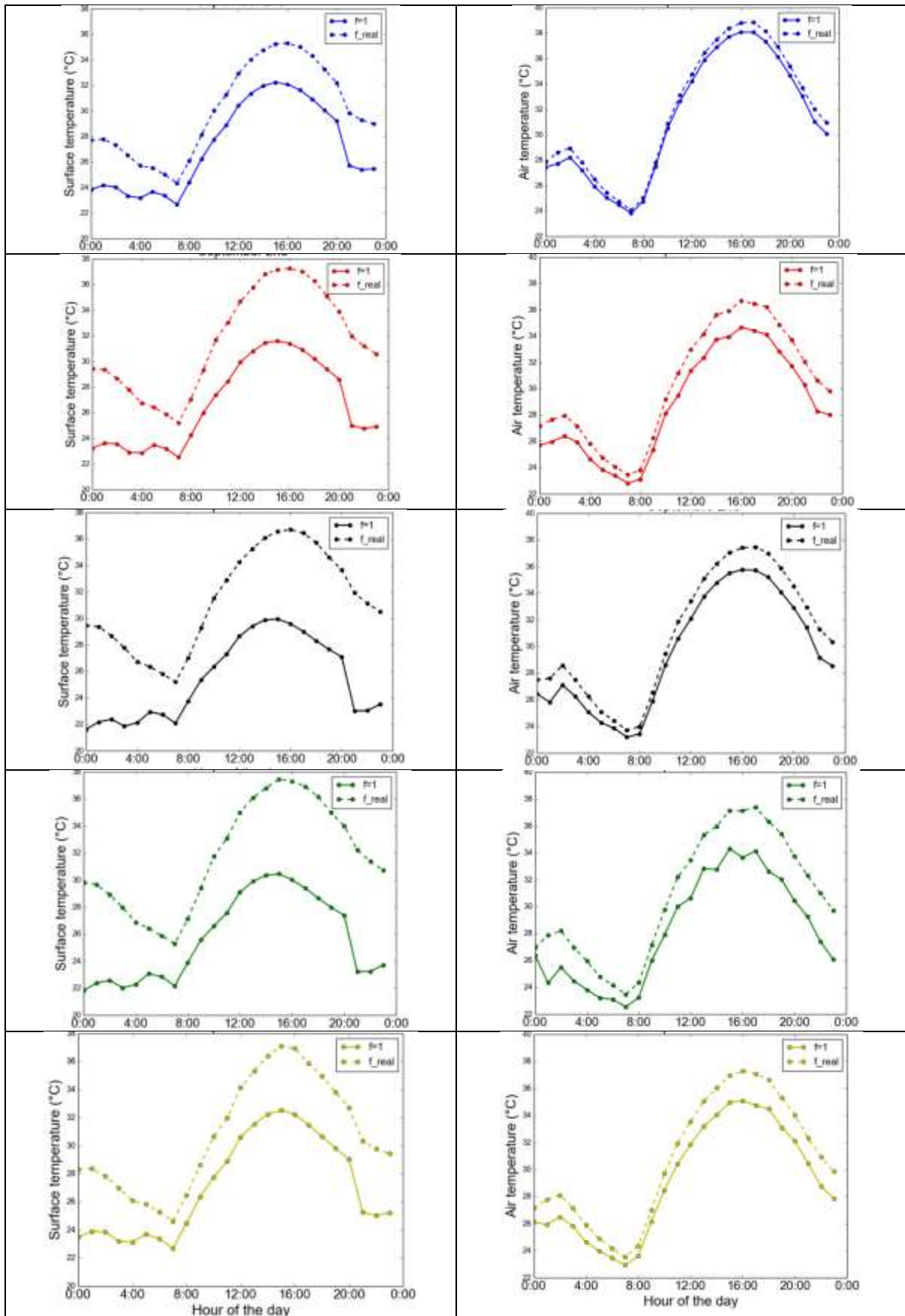


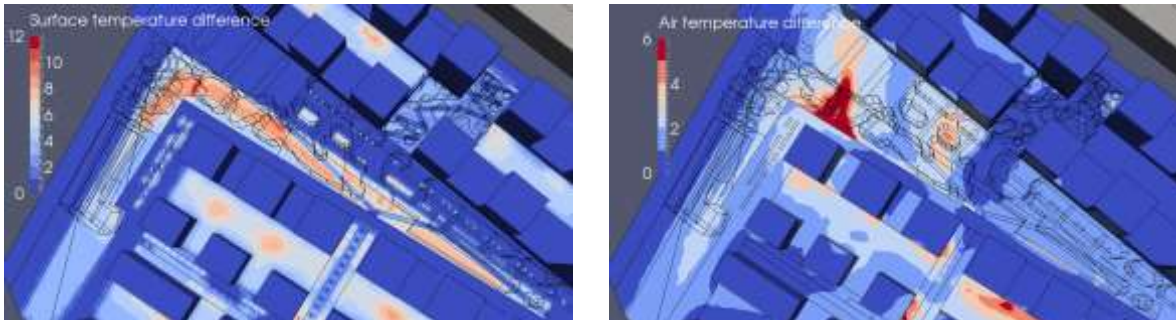
Figure 12: Surface and air temperature of green zones for the maximal water availability scenario for the 2nd Sept 2050

All surface temperatures become higher with water restriction events (Figure 13 and Figure 14). Zone 1 which was initially the warmest, becomes the coolest, whereas zones 3 and 4 at first cooler become as warm as zone 2 and 5. Surface temperature of zone 1 increases by 3°C, whereas for zone 3 and 4 it increases by 6°C in average, and by 2-5°C for zone 2 in average. Of course, this is due to the water availability, more reduced for zones 2, 3 and 4 than for zones 1 and 2. For zone 5, the temperature increases by 3.5°C.



1
2 Figure 13: Surface temperature (left) and air temperature (right) for each zone (from 1 at the top to 5 at the bottom) and for the two scenarios: full water availability ($f = 1$) and real water availability ($f = \text{real}$) for the 2nd Sept 2050

1 At 2 pm, when the impact is the highest, zones 3 and 4 show the highest surface temperature
2 differences: 2 to 7°C for the lawn and the perennial plants, 4 to 12°C for the forest border. On
3 these two zones evapotranspiration is only 20 to 25% of the maximal evapotranspiration rate.
4 On the opposite, zone 1 and 5 are moderately influenced with a maximum difference of 4°C.
5



6 *Figure 14: Surface temperature difference (left) and air temperature difference (right) for the Mail Finot between the two*
7 *configurations ($f = 1$ and $f = \text{real}$) at 2 pm the 2nd Sept 2050*

8 Concerning air temperature, a limit of the model can first be pointed out: the air
9 masses stagnate over the areas without dissipation and seems to stay in contact too much time
10 with the cooler surfaces. This cooling is less important when the real availability of water is
11 considered and the highest differences concentrate around the zones where air recirculation
12 occurs (Figure 14). However, the water stress still induces an increase of temperature in the
13 other areas. This increase is about 2°C but differs between each zone. With a full water
14 availability, zone 1 presents the highest air temperature and zone 5 is much cooler while the
15 surface temperatures between both zones are similar (Figure 13). This is due to the
16 accumulation of the cold air through its contact with vegetation and the cooling effect of the
17 dense forest on zone 5. Zone 2 is cooler than zone 3, due to the air circulation through the
18 cooler parts. The cooling in zone 4 is conditioned by the important air recirculation occurring.
19 However, considering the real water availability results in higher air temperatures and
20 attenuates the differences between zones. In average, zone 1 presents a lower cooling of 0.6°C
21 while zones 2, 3 and 5 are cooled down by 1.3-1.6°C. The dynamical behaviour is always
22 similar: during night, the differences get lower due to the low evapotranspiration. During
23 daytime, when solar radiation gets higher and surface temperatures increase,
24 evapotranspiration gets higher, and the water limitation affects the air temperature difference
25 between the two configurations.

26 4 Conclusions

27
28 This paper presents an original method coupling a hydrological model and the
29 commonly used Solene-Microclimat urban microclimate model to study the impact of water
30 stress on evapotranspiration and temperature at the district scale. The hydrological model,
31 MARIE was adapted from the URBS model (Pophillat et al, 2021) for the need of this study.
32 The coupling between the two models is introduced at different levels of the simulation: local
33 solar radiation, simulated by Solene-Microclimat, is used to calculate potential
34 evapotranspiration (PET) in MARIE; actual evapotranspiration (AET), simulated in detail
35 with MARIE by taking into account the water stress, is given as an input to Solene-
36 Microclimat. This 3-steps coupling approach is applied on an urban project, with a focus on
37 5 different green zones of a landscaped plaza and under future climate conditions (2050
38 scenario). The importance of considering water availability in microclimate simulation is
39 assessed by comparing surface and air temperature results obtained using PET instead of AET
40 in Solene-Microclimat.

1 Implementing the complete coupling approach at the district scale involves various
 2 challenges. First, both models detail numerous physical processes affecting the hydrological
 3 and microclimate conditions, and thus require a thorough parametrisation . The construction
 4 of the 3D mock-up in the microclimate model is also a crucial and fastidious step. Similarly,
 5 coupling the time and spatial scales of both model is often touchy: the hydrological simulation
 6 are performed during one year, taking into account the seasonal variation of the water
 7 availability and providing a robust estimation of the water stress during the summer period,
 8 and the 3D realistic urban forms are considered in the microclimate simulations with a high
 9 spatial resolution, allowing to take into account the buildings' shade and obstacle to wind.

10 Simulation results indicate that, for the case study, the water stress of green zones has
 11 a significant impact on vegetated surface temperature, with a mean of +4.7°C (between 3 and
 12 6°C) for a particular hot day, and a lower but yet significant effect on air temperature between
 13 0.6-1.6°C, over the studied area (Table 6).
 14

	Zone 1	Zone 2	Zone 3	Zone 4	Zone 5
Green areas surface T°	+3°C	+5°C	+6°C	+6°C	+3.5°C
Green areas air T°	+0.6°C	+1.6°C	+1.6°C	-	+1.6°C

15 *Table 6: Differences between the configurations with and without water-stress on surface and air temperature (for each*
 16 *green zones of the Mail Finot, 2nd september 2050 ; results in air temperature for the zone 4 is not realistic due to an*
 17 *inappropriate wind redistribution simulated)*

18 Simulations also evidence the strong variability of the hydrologic and microclimate conditions
 19 between and within each zone, especially on high and low strata and at the annual scale or
 20 during the hot period. This variability is analysed in the article, and numerous determining
 21 factors are identified: wind conditions, hydrogeological context (upstream runoff and water
 22 table depth), vegetation characteristics and exposition to solar radiation being the more
 23 significant.

24 As a perspective, further efforts should probably focus on the evaluation of the
 25 coupling approach. Here, simulation results have not been compared with observations on the
 26 case study (layout project and future climate conditions). Both models have been validated in
 27 previous studies under different conditions and on different variables (see the numerous
 28 references in the presentation section of the models). Nevertheless, applying the entire
 29 coupling approach on a case study with observations would be an interesting future step. This
 30 evaluation should confirm some assumptions and choices made in the approach, including the
 31 use of f ratio as the link between both models. First, f values are certainly very sensitive to the
 32 soil moisture extraction function in MARIE (Feddes law in Eq.10) which only provides a very
 33 simplified description of the root extraction process (Braud et al., 2005). Second, it is
 34 assumed that f is the same in the two models ; if this assumptions may be acceptable in the
 35 case of low strata (MARIE and Solene-Microclimat calculate PET by the same Pennan-
 36 Monteith equation), the approach is more questionable for the trees as in Solene-Microclimat,
 37 a volumetric PET is computed from a humidity gradient over a 3D representation of the tree
 38 crowns. Finally, the coupling approach adopted here is similar to a 'one-way data transfer'
 39 coupling (Brandmeyer and Karimi, 2000) with the modellers interacting with each model and
 40 operating manual transfers data between the two models. A higher level of coupling
 41 (automated data transfer, one model embedded in other, ...) **would require significant**
 42 **modifications of each source code. Based on the encouraging results of this study, such efforts**
 43 **could be undertaken in the future.**
 44

45 Funding

46 This work was supported by the SOLIDEO, the Olympic Delivery Authority of the Paris
 47 olympic games in 2024 [grant number 2019 000 19].

1
2
3
4
5
6
7
8
9
10
11
12
13
14
15
16
17
18
19
20
21
22
23
24
25
26
27
28
29
30
31
32
33
34
35
36
37
38
39
40
41
42
43
44
45
46
47
48
49
50

References

Allen, R.G., Pereira, L.S., Raes, D., Smith, M., 1998. Crop evapotranspiration (guidelines for computing crop water requirements) (FAO Irrigation and Drainage Paper No. 56). FAO, Rome.

Athamena, K., 2012. Modélisation et simulation des microclimats urbains : étude de l'impact de la morphologie urbaine sur le confort dans les espaces extérieurs : cas des éco-quartiers (PhD thesis). Ecole centrale de Nantes, Nantes, France.

Azam, M.-H., Morille, B., Bernard, J., Musy, M., Rodriguez, F., 2018. A new urban soil model for SOLENE-microclimat: Review, sensitivity analysis and validation on a car park. *Urban Climate* 24, 728–746. <https://doi.org/10.1016/j.uclim.2017.08.010>

Berthier, E., Dupont, S., Mestayer, P.G., Andrieu, H., 2006. Comparison of two evapotranspiration schemes on a sub-urban site. *Journal of Hydrology* 328, 635–646. <https://doi.org/10.1016/j.jhydrol.2006.01.007>

Berthier, E., Sage, J., Dumont, E., Mosini, M.-L., Rodriguez, F., Toriel, M., 2020. Assessing the impact of the development of an urban district on shallow groundwater using the integrated urban hydrological model URBS (No. EGU2020-10436). Presented at the EGU2020, Copernicus Meetings. <https://doi.org/10.5194/egusphere-egu2020-10436>

Bouyer, J., 2009. Modélisation et simulation des microclimats urbains - Étude de l'impact de l'aménagement urbain sur les consommations énergétiques des bâtiments (PhD thesis). Université de Nantes, Nantes, France.

Brandmeyer, J.E., Karimi, H.A., 2000. Coupling methodologies for environmental models. *Environmental Modelling & Software* 15, 479–488. [https://doi.org/10.1016/S1364-8152\(00\)00027-X](https://doi.org/10.1016/S1364-8152(00)00027-X)

Braud, I., Varado, N., Olioso, A., 2005. Comparison of root water uptake modules using either the surface energy balance or potential transpiration. *Journal of Hydrology* 301, 267–286. <https://doi.org/10.1016/j.jhydrol.2004.06.033>

Breuer, L., Eckhardt, K., Frede, H.-G., 2003. Plant parameter values for models in temperate climates. *Ecological Modelling* 169, 237–293. [https://doi.org/10.1016/S0304-3800\(03\)00274-6](https://doi.org/10.1016/S0304-3800(03)00274-6)

Broadbent, A.M., Coutts, A.M., Tapper, N.J., Demuzere, M., 2018. The cooling effect of irrigation on urban microclimate during heatwave conditions. *Urban Climate*, ICUC9: The 9th International Conference on Urban Climate 23, 309–329. <https://doi.org/10.1016/j.uclim.2017.05.002>

Broekhuizen, I., Muthanna, T.M., Leonhardt, G., Viklander, M., 2019. Urban drainage models for green areas: Structural differences and their effects on simulated runoff. *Journal of Hydrology X* 5, 100044. <https://doi.org/10.1016/j.hydroa.2019.100044>

Brooks, R.H., Corey, A.T., 1964. Hydraulic properties of porous media, *Hydrology papers* n°3. Colorado State University, Fort Collins.

Daniel, M., Lemonsu, A., Viguié, V., 2018. Role of watering practices in large-scale urban planning strategies to face the heat-wave risk in future climate. *Urban Climate*, ICUC9: The 9th International Conference on Urban Climate 23, 287–308. <https://doi.org/10.1016/j.uclim.2016.11.001>

DiGiovanni-White, K., Montalto, F., Gaffin, S., 2018. A comparative analysis of micrometeorological determinants of evapotranspiration rates within a heterogeneous urban environment. *Journal of Hydrology* 562, 223–243. <https://doi.org/10.1016/j.jhydrol.2018.04.067>

Eermak, J., 1998. Leaf distribution in large trees and stands of the floodplain forest in southern Moravia. *Tree Physiology* 18, 727–737. <https://doi.org/10.1093/treephys/18.11.727>

- 1 Eliáš, P., 1979. Stomatal oscillations in adult forest trees in natural environment. *Biol Plant*
2 21, 71–74. <https://doi.org/10.1007/BF02888722>
- 3 Feddes, R.A., Kowalik, P.J., Zaradny, H., 1978. *Simulation of Field Water Use and Crop*
4 *Yield*, Wiley. ed.
- 5 Grimmond, C.S.B., Oke, T.R., 1991. An Evapotranspiration-Interception Model for Urban
6 Areas. *Water Resour. Res.* 27, 1739–1755. <https://doi.org/10.1029/91WR00557>
- 7 Gromke, C., Blocken, B., Janssen, W., Merema, B., van Hooff, T., Timmermans, H., 2015.
8 CFD analysis of transpirational cooling by vegetation: Case study for specific
9 meteorological conditions during a heat wave in Arnhem, Netherlands. *Building and*
10 *Environment, Special Issue: Climate adaptation in cities* 83, 11–26.
11 <https://doi.org/10.1016/j.buildenv.2014.04.022>
- 12 Gyeveki, M., Hrotkó, K., Honfi, P., 2012. Comparison of leaf population of sweet cherry
13 (*Prunus avium* L.) trees on different rootstocks. *Scientia Horticulturae* 141, 30–36.
14 <https://doi.org/10.1016/j.scienta.2012.03.015>
- 15 IPCC, 2014. *Climate change 2014: Synthesis Report. Contribution of Working Groups I, II and*
16 *II to the Fifth Assessment Report of the Intergovernmental Panel on Climate Change*
17 [Core Writing Team, R.K. Pachauri and L.A. Meyer (eds.)]. IPCC, Geneva,
18 Switzerland.
- 19 Jankowfsky, S., Branger, F., Braud, I., Rodriguez, F., Debionne, S., Viallet, P., 2014.
20 Assessing anthropogenic influence on the hydrology of small peri-urban catchments:
21 Development of the object-oriented PUMMA model by integrating urban and rural
22 hydrological models. *Journal of Hydrology* 517, 1056–1071.
23 <https://doi.org/10.1016/j.jhydrol.2014.06.034>
- 24 Järvi, L., Grimmond, C.S.B., Christen, A., 2011. The Surface Urban Energy and Water
25 Balance Scheme (SUEWS): Evaluation in Los Angeles and Vancouver. *Journal of*
26 *Hydrology* 411, 219–237. <https://doi.org/10.1016/j.jhydrol.2011.10.001>
- 27 Koelbing, M., Schuetz, T., Weiler, M., 2021. Downscaling potential evapotranspiration to the
28 urban canyon. *Hydrology and Earth System Sciences. Discussions* [preprint].
29 <https://doi.org/10.5194/hess-2021-24>
- 30 Leconte, F., Bouyer, J., Claverie, R., 2020. Nocturnal cooling in Local Climate Zone:
31 Statistical approach using mobile measurements. *Urban Climate* 33, 100629.
32 <https://doi.org/10.1016/j.uclim.2020.100629>
- 33 Lindberg, F., Grimmond, C.S.B., Gabey, A., Huang, B., Kent, C.W., Sun, T., Theeuwes, N.E.,
34 Järvi, L., Ward, H.C., Capel-Timms, I., Chang, Y., Jonsson, P., Krave, N., Liu, D.,
35 Meyer, D., Olofson, K.F.G., Tan, J., Wästberg, D., Xue, L., Zhang, Z., 2018. Urban
36 Multi-scale Environmental Predictor (UMEP): An integrated tool for city-based
37 climate services. *Environmental Modelling & Software* 99, 70–87.
38 <https://doi.org/10.1016/j.envsoft.2017.09.020>
- 39 Lingling, Z., Jun, X., Chong-Yu, X., Zhonggen, W., Leszek, S., 2013. Evapotranspiration
40 estimation methods in hydrological models. *Journal of Geographical Sciences* 12.
41 <https://doi.org/10.5194/hess-2021-24>
- 42 Malys, L., 2012. *Évaluation des impacts directs et indirects des façades et des toitures*
43 *végétales sur le comportement thermique des bâtiments (PhD thesis)*. Ecole Centrale
44 de Nantes, Nantes, France.
- 45 Martilli, A., Krayenhoff, E.S., Nazarian, N., 2020. Is the Urban Heat Island intensity relevant
46 for heat mitigation studies? *Urban Climate* 31, 100541.
47 <https://doi.org/10.1016/j.uclim.2019.100541>
- 48 Masson, V., 2000. A Physically-Based Scheme For The Urban Energy Budget In
49 Atmospheric Models. *Boundary-Layer Meteorology* 94, 357–397.
50 <https://doi.org/10.1023/A:1002463829265>

- 1 Miguet, F., 2000. Paramètres physiques des ambiances architecturales : Un modèle numérique
2 pour la simulation de la lumière naturelle dans le projet urbain. (PhD thesis).
3 Université de Nantes, Nantes, France.
- 4 Miller, D.L., Alonzo, M., Roberts, D.A., Tague, C.L., McFadden, J.P., 2020. Drought
5 response of urban trees and turfgrass using airborne imaging spectroscopy. *Remote*
6 *Sensing of Environment* 240, 111646. <https://doi.org/10.1016/j.rse.2020.111646>
- 7 Musy, M., Azam, M.-H., Guernouti, S., Morille, B., Rodler, A., 2021. The SOLENE-
8 Microclimat Model: Potentiality for Comfort and Energy Studies, in: Palme, M.,
9 Salvati, A. (Eds.), *Urban Microclimate Modelling for Comfort and Energy Studies*.
10 Springer International Publishing, Cham, pp. 265–291. [https://doi.org/10.1007/978-3-](https://doi.org/10.1007/978-3-030-65421-4_13)
11 [030-65421-4_13](https://doi.org/10.1007/978-3-030-65421-4_13)
- 12 Musy, M., Malys, L., Morille, B., Inard, C., 2015. The use of SOLENE-microclimat model to
13 assess adaptation strategies at the district scale. *Urban Climate, Cooling Heat Islands*
14 14, 213–223. <https://doi.org/10.1016/j.uclim.2015.07.004>
- 15 Oke, T.R., 1982. The energetic basis of the urban heat island. *Q.J Royal Met. Soc.* 108, 1–24.
16 <https://doi.org/10.1002/qj.49710845502>
- 17 Pophillat, W., Sage, J., Rodriguez, F., Braud, I., 2021. Dealing with shallow groundwater
18 contexts for the modelling of urban hydrology – A simplified approach to represent
19 interactions between surface hydrology, groundwater and underground structures in
20 hydrological models. *Environmental Modelling & Software* 144, 105144.
21 <https://doi.org/10.1016/j.envsoft.2021.105144>
- 22 Rawls, W.J., Brakensiek, L., Saxton, E., 1982. Estimation of soil water properties.
23 *Transactions of the ASAE* 25, 1316–1320.
- 24 Robitu, M., 2005. Étude de l’interaction entre le bâtiment et son environnement urbain :
25 influence sur les conditions de confort en espaces extérieurs (PhD thesis). Université
26 de Nantes, Nantes, France.
- 27 Rodler, A., Guernouti, S., Musy, M., Bouyer, J., 2018. Thermal behaviour of a building in its
28 environment: Modelling, experimentation, and comparison. *Energy and Buildings*
29 168, 19–34. <https://doi.org/10.1016/j.enbuild.2018.03.008>
- 30 Rodriguez, F., Andrieu, H., Morena, F., 2008. A distributed hydrological model for urbanized
31 areas – Model development and application to case studies. *Journal of Hydrology* 351,
32 268–287. <https://doi.org/10.1016/j.jhydrol.2007.12.007>
- 33 Saaroni, H., Amorim, J.H., Hiemstra, J.A., Pearlmutter, D., 2018. Urban Green Infrastructure
34 as a tool for urban heat mitigation: Survey of research methodologies and findings
35 across different climatic regions. *Urban Climate* 24, 94–110.
36 <https://doi.org/10.1016/j.uclim.2018.02.001>
- 37 Sample, J.D., Heaney, P.J., 2006. Integrated Management of Irrigation and Urban Storm-
38 Water Infiltration. *Journal of Water Resources Planning and Management* 132, 362–
39 373. [https://doi.org/10.1061/\(ASCE\)0733-9496\(2006\)132:5\(362\)](https://doi.org/10.1061/(ASCE)0733-9496(2006)132:5(362))
- 40 Samson, R., Provoost, S., Willaert, L., Lemeur, R., 2005. Supporting dune management by
41 quantitative estimation of evapotranspiration, in: Herrier, J.-L., Mees, J., Salman, A.,
42 Seys, J., Van Nieuwenhuysse, H., Dobbelaere, I. (Eds.), *Proceedings “Dunes and*
43 *Estuaries 2005.”* VLIZ Special Publication 19, Koksijde, Belgium, pp. 345–354.
- 44 Santamouris, M., 2014. On the energy impact of urban heat island and global warming on
45 buildings. *Energy and Buildings* 82, 100–113.
46 <https://doi.org/10.1016/j.enbuild.2014.07.022>
- 47 Shashua-Bar, L., Hoffman, M.E., 2004. Quantitative evaluation of passive cooling of the UCL
48 microclimate in hot regions in summer, case study: urban streets and courtyards with
49 trees. *Building and Environment* 39, 1087–1099.
50 <https://doi.org/10.1016/j.buildenv.2003.11.007>

1 Simunek, J., Sejna, M., Saito, H., Sakai, M., van Genuchten, M.Th., 2013. The HYDRUS-1D
2 software package for simulating the one-dimensional movement of water, heat and
3 multiple solutes in variably-saturated media (HYDRUS Software Series 3 No. Version
4 4.17). Departement of Environmental Sciences, University of California Riverside,
5 Riverside, California, USA.

6 Stavropoulos-Laffaille, X., Chancibault, K., Andrieu, H., Lemonsu, A., Masson, V., 2019.
7 Coupling Urban Water and Energy Budgets with TEB-Hydro: Case Study on the
8 French Catchment Pin Sec, in: Mannina, G. (Ed.), New Trends in Urban Drainage
9 Modelling, Green Energy and Technology. Springer International Publishing, Cham,
10 pp. 734–739. https://doi.org/10.1007/978-3-319-99867-1_127

11 Tabares-Velasco, P.C., Srebric, J., 2011. Experimental quantification of heat and mass
12 transfer process through vegetated roof samples in a new laboratory setup.
13 International Journal of Heat and Mass Transfer 54, 5149–5162.
14 <https://doi.org/10.1016/j.ijheatmasstransfer.2011.08.034>

15 U.S. Environmental Protection Agency, 2008. Reducing Urban Heat Islands: Compendium of
16 Strategies. Draft. <https://www.epa.gov/heat-islands/heat-island-compendium>

17 Wang, T., Tigerstedt, P.M.A., Vihera-Aarnio, A., 1995. Photosynthesis and canopy
18 characteristics in genetically defined families of silver birch (*Betula pendula*). Tree
19 Physiology 15, 665–671. <https://doi.org/10.1093/treephys/15.10.665>

20 Zhao, L., Xia, J., Xu, C., Wang, Z., Sobkowiak, L., Long, C., 2013. Evapotranspiration
21 estimation methods in hydrological models. Journal of Geographical Sciences 23,
22 359–369. <https://doi.org/10.1007/s11442-013-1015-9>

24 Appendix

25

Surface type	Albedo	Emissivity	Transmittance	Surface composition	
				Material	Thickness (m)
Wall	0.65	0.9	0	OSB panel	0.011
				Wood wool	0.22
				OSB panel	0.011
				Lime	0.018
Roof	0.35	0.9	0	OSB panel	0.22
				External insulation	0.25
				Cellulose wadding	0.04
				Wooden panel	0.5
Drainage ditch	0.3	0.9	0	Soil	0.7
Wooden path	0.25	0.9	0	Wood	0.026
				Soil	0.674
Lawn	0.25	0.9	0.2	Soil	0.7
Concrete pavement	0.45	0.9	0	Concrete	0.3
				Gravel	0.15
				Soil	0.25
Courtyard	0.25	0.9	0	Soil	0.7
Trees	0.3	0.97	0.2	-	-
Perennial plant	0.3	0.9	0.2	-	-
Road	0.17	0.9	0	Asphalt	0.05
				Gravel	0.25
				Soil	0.4
Forest border	0.3	0.9	0.2	Soil	0.7

26

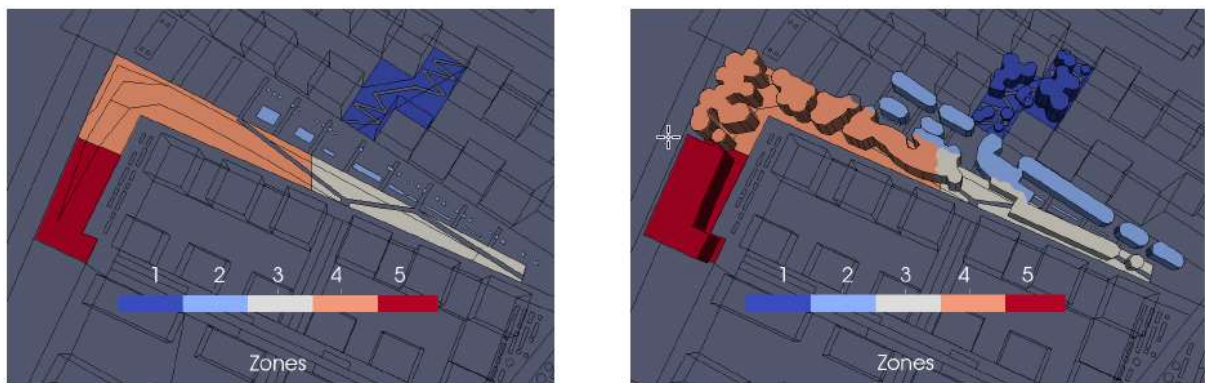
Table A.1: Thermal and radiative properties of the surfaces in the Solene-Microclimat model

1

	Conductivity [W/mK]	Thermal capacity [J/kgK]	Density [kg/m ³]
Wooden path wood	0.14	1880	600
Asphalt	0.75	950	2100
Soil	0.7	900	1600
Gravel	2	1045	1950
Concrete	1.65	1000	2500
Cellulose wadding	0.045	1400	55
Wood wool	0.04	1200	250
Wooden panel	0.083	2090	406
External insulation	0.037	1550	143
OSB panel	0.13	1692	650
Lime	0.333	800	850

2

Table A.2: Thermal properties of the materials in the Solene-Microclimat model



3

4

Figure A.1: Delimitation of the five zones for the low (left) and high (right) stratum in the Solene-Microclimat model

5

6

7

8

9